FEMS Microbiology Ecology, 2024, 100, fiae110
DOI: 10.1093/femsec/fiae110
Advance access publication date: 7 August 2024
Research Article

Single-cell measurement of microbial growth rate with Raman microspectroscopy

Tristan A. Caro [1,*], Srishti Kashyap[1], George Brown[2], Claudia Chen[2], Sebastian H. Kopf[1], Alexis S. Templeton[1]

[1]Department of Geological Sciences, University of Colorado Boulder, Boulder, CO 80309, United States
[2]Department of Applied Mathematics, University of Colorado Boulder, Boulder, CO 80309, United States
*Corresponding author. Department of Geological Sciences, University of Colorado Boulder, 2200 Colorado Ave, Benson Earth Sciences Building, Rm. 285. UCB 399, Boulder, CO 80309, United States. E-mail: tristan.caro@colorado.edu
Editor: [Tillmann Lueders]

Abstract

Rates of microbial growth are fundamental to understanding environmental geochemistry and ecology. However, measuring the heterogeneity of microbial activity at the single-cell level, especially within complex populations and environmental matrices, remains a forefront challenge. Stable isotope probing (SIP) is a method for assessing microbial growth and involves measuring the incorporation of an isotopic label into microbial biomass. Here, we assess Raman microspectroscopy as a SIP technique, specifically focusing on the measurement of deuterium (^{2}H), a tracer of microbial biomass production. We correlatively measured cells grown in varying concentrations of deuterated water with both Raman spectroscopy and nanoscale secondary ion mass spectrometry (nanoSIMS), generating isotopic calibrations of microbial ^{2}H. Relative to Raman, we find that nanoSIMS measurements of ^{2}H are subject to substantial dilution due to rapid exchange of H during sample washing. We apply our Raman-derived calibration to a numerical model of microbial growth, explicitly parameterizing the factors controlling growth rate quantification and demonstrating that Raman–SIP can sensitively measure the growth of microorganisms with doubling times ranging from hours to years. The measurement of single-cell growth with Raman spectroscopy, a rapid, nondestructive technique, represents an important step toward application of single-cell analysis into complex sample matrices or cellular assemblages.

Keywords: deuterium; growth rate; nanoSIMS; Raman microspectroscopy; single-cell analysis; stable isotope probing

Introduction

Microbial growth rate is a critical parameter for assessing biogeochemical cycling, environmental habitability, and microbial fitness. Not only does the rate of microbial growth represent a chemical process, but it is also a parameter that microorganisms modulate in response to changing conditions: microorganisms may more readily replicate when conditions are favorable to them and adopt alternative physiologic states under adverse conditions.

Methods for measuring microbial growth often rely upon the addition of an isotopically labeled substrate to a natural sample and measuring its incorporation into microbial biomass, a method generally termed stable isotope probing (SIP) (Dumont and Murrell 2005, Hungate et al. 2015, Caro et al. 2023). SIP has been applied with the stable isotopes of various elements including H, C, N, O, S, and so on, through measurement of single-cells (Eichorst et al. 2015, Berry et al. 2015, Trembath-Reichert et al. 2017, 2021, Cui et al. 2019), membrane lipids (Kopf et al. 2015, Wegener et al. 2016, Caro et al. 2023), and nucleic acids (Hungate et al. 2015, Koch et al. 2018, Coskun et al. 2019, Li et al. 2019). One approach to probe cellular biosynthesis is to amend an environmental sample with deuterated water (^2H_2O) (Morono et al. 2011, Kellermann et al. 2012, Eichorst et al. 2015, Kopf et al. 2015, Trembath-Reichert et al. 2017, Schaible et al. 2022, Caro et al. 2023). Water is incorporated into microbial biomass during the synthesis of lipids, nucleic acids, and proteins, and so probing a sample with deuterated water allows the quantification of microbial biomass growth. ^2H_2O has been termed a "passive" tracer for microbial anabolism, as it is nutritionally neutral and taxonomically agnostic.

In microbial communities, spatial relationships dictate ecological and evolutionary dynamics, as well as community structure and function (Boetius et al. 2000, Cordero et al. 2012, Marlow et al. 2021, Sokol et al. 2022, Védère et al. 2022). Microbial growth is known to be extremely heterogenous in environments such as soil matrices (Sokol et al. 2022), marine particles, (Grossart et al. 2003, Kirchman 2016, Ebrahimi et al. 2019), the rock-hosted subsurface (Casar et al. 2020, Templeton and Caro 2023), and others. Spatially resolved measurements of microbial growth can identify the habitability and biological activity of environmental samples at the microscale. Furthermore, single-cell measurements of microbial growth are especially useful for microbial ecologists as they provide information on anabolic heterogeneity across and within populations. However, describing the spatial distributions and intracommunity heterogeneity of microorganisms in the environment remains one of the primary challenges in microbial ecology.

Currently, nanoscale secondary ion mass spectrometry (nanoSIMS) is a primary method with which single-cell isotopic ratios have been reported in natural samples (Morono et al. 2011, Kopf et al. 2015, Dekas et al. 2019, Schaible et al. 2022). A nanoSIMS instrument applies a primary ion beam (Cs^+) to ionize and ablate a sample, inducing the release of secondary ions whose isotopic composition is measured by magnetic sector isotope ratio mass spectrometry. NanoSIMS has many benefits

Received 22 January 2024; **revised** 12 July 2024; **accepted** 5 August 2024

as an analytical technique: it can measure multiple isotopes simultaneously and allows elemental and isotopic imaging at the nanoscale. However, nanoSIMS is a destructive technique, often requiring metallic sputtering and can result in the complete ablation of a cell, and so is typically considered an end-point analysis (Schaible et al. 2022). NanoSIMS is also extremely intensive in terms of time, resources, and operating cost, and only a handful of instruments exist in North America and Europe (CAMECA, 2024). Given these limitations, it would be useful to have additional methods that can complement the strengths of nanoSIMS while overcoming some of its drawbacks. We therefore set out to assess alternative single-cell methodologies.

In 2015, foundational work by Berry et al. (2015) established Raman microscale spectroscopy ("microspectroscopy") as a viable tool for detecting deuterium (^2H) enrichment of microbial biomass at the single-cell level. Raman-based measurements of deuterium in microbial biomass rely on the principle that Raman scattering of light (in this case, monochromatic 532 nm "green" light) by carbon–hydrogen bonds generates a strong spectral band centered at 2800 cm^{-1}, corresponding to C–H bonding environments associated with lipids, proteins, and nucleic acids of cells. When deuterium is incorporated into microbial biomass as C–^2H ("C–D") bonds, this band becomes red-shifted to 2200 cm^{-1} (Fig. 1B). In previous work, this "CD% metric", defined as the fractional abundance of CD and CH peak areas, [CD% = CD/(CD + CH) × 100%] was found to correlate with the deuterium fractional abundance (^2F) of the growth medium provided to the organisms (Berry et al. 2015). Berry et al. (2015) illustrated applications of Raman–SIP in combination with fluorescence *in situ* hybridization (FISH) and cell-sorting methodologies to capture the identity of active microbial community members.

For our study, we built upon this prior work in four key aspects. First, we use cultured representatives of two environmentally relevant anaerobic taxa to generate a robust hydrogen isotopic calibration for Raman spectroscopy (Fig. 2). Second, we combined the results of our isotopic calibration with a numerical model of microbial growth to evaluate the feasibility and sensitivity of Raman–SIP for quantitative inference of microbial biomass growth rate (Fig. 3). Third, the cells used to generate our Raman-based isotopic calibration were correlatively measured by nanoSIMS to determine the extent to which nanoSIMS and Raman-based measurements agree. Finally, we provide a computational framework and graphical user interface (GUI) for Raman–SIP that allows users to optimize SIP incubations for their specific study system.

Materials and methods

Microorganisms and growth conditions

We cultivated *Thermodesulfovibrio hydrogeniphilus* (Haouari et al. 2008) and *Methanobacterium NSHQ04* (Miller et al. 2018), in media containing 0%, 10%, 20%, 30%, 40%, or 50% ^2H_2O (0% = local ultrapure water which contains ~140 ppm ^2H_2O naturally). Base media (described below) were modified with different percentages (v/v) of ^2H_2O (Cambridge Isotope Laboratories), depending on the final isotopic enrichment desired for the experiment. All cultures were grown in the dark in anaerobic 60 ml serum vials containing 25 ml of growth medium.

Thermodesulfovibrio hydrogeniphilus HBr5^T (DSM 18151) (Haouari et al. 2008), a sulfate-reducing bacterium (SRB), was obtained from the Deutsche Sammlung von Mikroorganismen und Zellkulturen. It was grown in a modified DSM 641 medium that contained (per liter): 1.0 g NH_4Cl, 2.0 g Na_2SO_4, 1.0 g $Na_2S_2O_3 \times 5H_2O$, 1.0 g $MgSO_4 \times 7H_2O$, 0.1 g $CaCl_2 \times 2H_2O$, 0.5 g KH_2PO_4, 2.0 g $NaHCO_3$, 1 ml trace element solution SL-10, 1 ml selenite–tungstate solution, 1 g yeast extract, 0.5 ml sodium resazurin (0.1% w/v), 0.2 g sodium acetate, 10 ml 141 vitamin solution, and 0.1 g $Na_2S \times 9H_2O$. The headspace was flushed and over-pressurized with 1 bar H_2:CO_2 (80:20).

Methanobacterium NSHQ04 (Miller et al. 2018) is a methanogenic archaeon enriched from groundwater isolated from the Samail ophiolite in Oman. The culture was grown in a synthetic site water (NSHQ04) medium (Miller et al. 2018) containing (per liter): 420 mg NaCl, 683 mg $CaCl_2 \times 2H_2O$, 1.2 mg H_4SiO_4, 1.7 mg NaBr, 60 mg $MgCl_2 \times 6H_2O$, 100 mg NH_4Cl, 10 ml 141 trace elements, 10 ml 141 vitamins, 0.5 ml sodium resazurin (0.1 w/v), 20 ml antibiotic cocktail [containing per 100 ml MilliQ water, 500 mg penicillin G, 500 mg streptomycin, 500ul ampicillin (10 mg ml^{-1} stock)], 10 ml KH_2PO_4 (1.1 w/v), 4 ml yeast extract (5% w/v), 2 ml $Fe(NH_4)_2(SO_4)_2$ (0.2% w/v), 10 ml sodium formate (100 mM), 10 ml cysteine–HCl (2.5% w/v), and 10 ml Na_2S (2.5% w/v). The headspace was flushed and over-pressurized with 2 bar H_2:N_2 (5:95).

Cultures of *T. hydrogeniphilus* and *M. NSHQ04* were incubated in forced-air incubators at 65°C and 40°C, respectively. Cultures were transferred three times into media of identical deuterium enrichment. Before each transfer, cultures were grown to stationary phase, which was reached in 3–4 days for *T. hydrogeniphilus* and 12–14 days for *Methanobacterium NSHQ04*. This ensured that the cells measured were at or near isotopic equilibrium with their respective growth water. After the third transfer, 1 ml of each culture was harvested and fixed by addition of paraformaldehyde to a final concentration of 2% (v/v). Fixed cells were washed by centrifugation in successively dilute phosphate-buffered saline (PBS) of rinses [1X, 1%, 0.1%, and 0.01% (v/v) PBS] to ensure the removal of excess salts and fixative. PBS was composed of Dulbecco's formula: KCl 200 mg l^{-1}, KH_2PO_4 200 mg l^{-1}, NaCl 8000 mg l^{-1}, Na_2HPO_4 1150 mg l^{-1}. After the final wash, cells were resuspended in 50 µl of 0.01% (v/v) PBS.

Sample preparation

Sample coupons were prepared by raster engraving of aluminum-coated glass slides (Deposition Research Lab Inc.) with an Epilog Mini 24 CO_2 laser machine operating at 80 W laser power, 10% etching speed, to create a 3 × 6 grid. These etchings were used to manually break the glass slide, producing 7 mm^2 coupons that are compatible with both Raman and nanoSIMS sample mounts. Aluminum coupons were used instead of silicon wafers (often used for nanoSIMS studies) because silicon exhibits a large peak at 520 cm^{-1} in the Raman spectrum. All coupons were sterilized and rendered organic-clean by combustion for 8 h at 450°C in a muffle furnace. 5 µl of fixed and washed cells was spotted on individual coupons and allowed to air-dry.

Raman spectroscopy, fitting, and SIP calculations

Raman spectroscopy was conducted at the Raman Microspectroscopy Laboratory, Department of Geological Sciences, University of Colorado-Boulder (RRID:SCR_019305) on a Horiba LabRAM HR Evolution Raman spectrometer equipped with a 100 mW 532 nm excitation laser. The laser was focused with a 100X (NA = 0.90) air objective lens, resulting in a spot size of ~1 µm. Single-cell spectra were captured in the 200–3150 cm^{-1} range using 100% laser power (2.55 mW) over 2 acquisitions of 45 s. We note that, at time of analysis, the laser employed here was near end-of-life, thereby requiring relatively long acquisition times (45 s). After the collection of the original dataset a new laser was installed, which

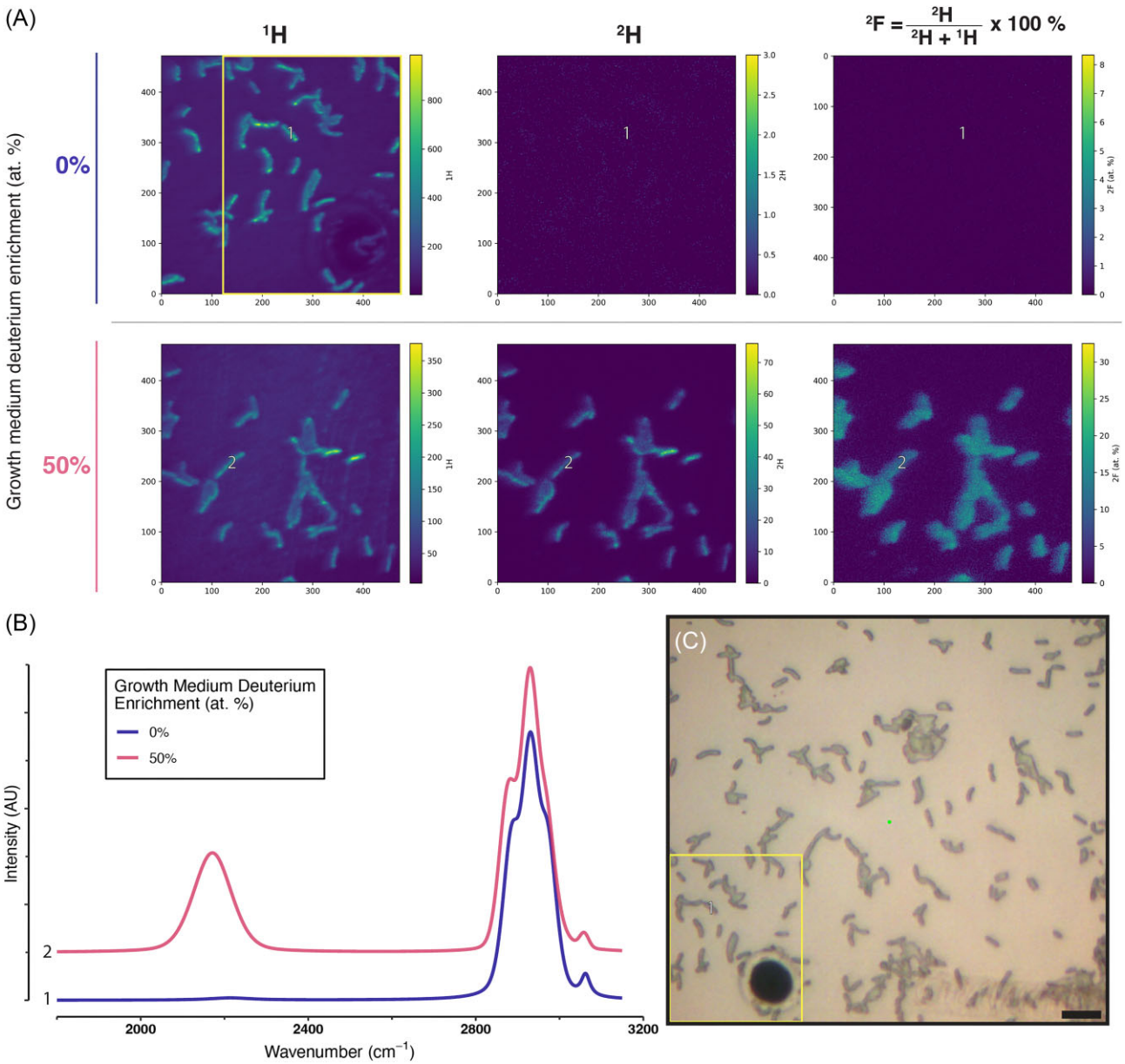

Figure 1. Representative Raman and nanoSIMS data collected in this study. Across all panels data from two representative cells, "1" and "2," are noted. Representative nanoSIMS isotopic images of are shown in Panel A, with pixel counts labeled on the x- and y-axes. From left to right, the pixel intensity in each panel corresponds to direct ion counts for $^1H^-$, $^2H^-$, and the fractional abundance of deuterium (^2F), respectively. The top row shows cells grown in 0% ^2H_2O (natural abundance); the bottom row displays cells grown in 50 at. % ^2H_2O. Representative single-cell fitted Raman spectra are shown in Panel B, with the characteristic C–H band between 2800 and 3000 cm^{-1} visible. For cells grown in deuterated media (Cell 2), the C–D band emerges between 2040 and 2300 cm^{-1}. Panel C displays a typical micrograph captured through a confocal Raman microspectroscope. The scale bar represents 2 μm. Cells in all panels are *Thermodesulfovibrio hydrogeniphilus*. The boxes annotated Panels A and C represent a correlated region imaged with nanoSIMS and Raman (reflected light), respectively.

resulted in acquisition times of 10 s at 10% laser power. Future researchers attempting to replicate our methods should note the effective laser power of their instrument and adjust acquisition time accordingly.

A 100 μm confocal pinhole and 600 lines mm^{-1} diffraction grating were used, resulting in a spectral resolution of ~4.5 cm^{-1}. Duplicate acquisitions were averaged to remove noise and cosmic ray spikes. Spectra were baseline-subtracted using a polynomial fit in LabSpec 6 (Horiba Scientific). Fitting of bands in the 1800–3150 cm^{-1} region was performed using Gaussian–Lorentzian curve fitting algorithms to integrate C–D (2040–2300 cm^{-1}) and C–H (2800–3100 cm^{-1}) bands. Raman-derived ^2F was determined by calculating the CD% value of each spectrum: $^2F = CD\% = CD/(CH + CD) \times 100\%$ where CD and CH are the areas of the C–D and C–H bands, respectively.

To correlate Raman spectra with nanoSIMS data, extensive context maps of the sample coupons were acquired using reflected light microscopy on the Raman instrument. Before cell spotting, fiducial markings were etched into the aluminum coupon surface with a Leica LMD7000 microdissection system.

As described in the section "Results and Discussion," modeling of growth rate was carried out with Eqs (1–3). (Kopf et al. 2016, Caro et al. 2023). Using these formulae, we modeled μ across a range of F_L, t, and a_w. We define an acceptable cutoff using a relative error

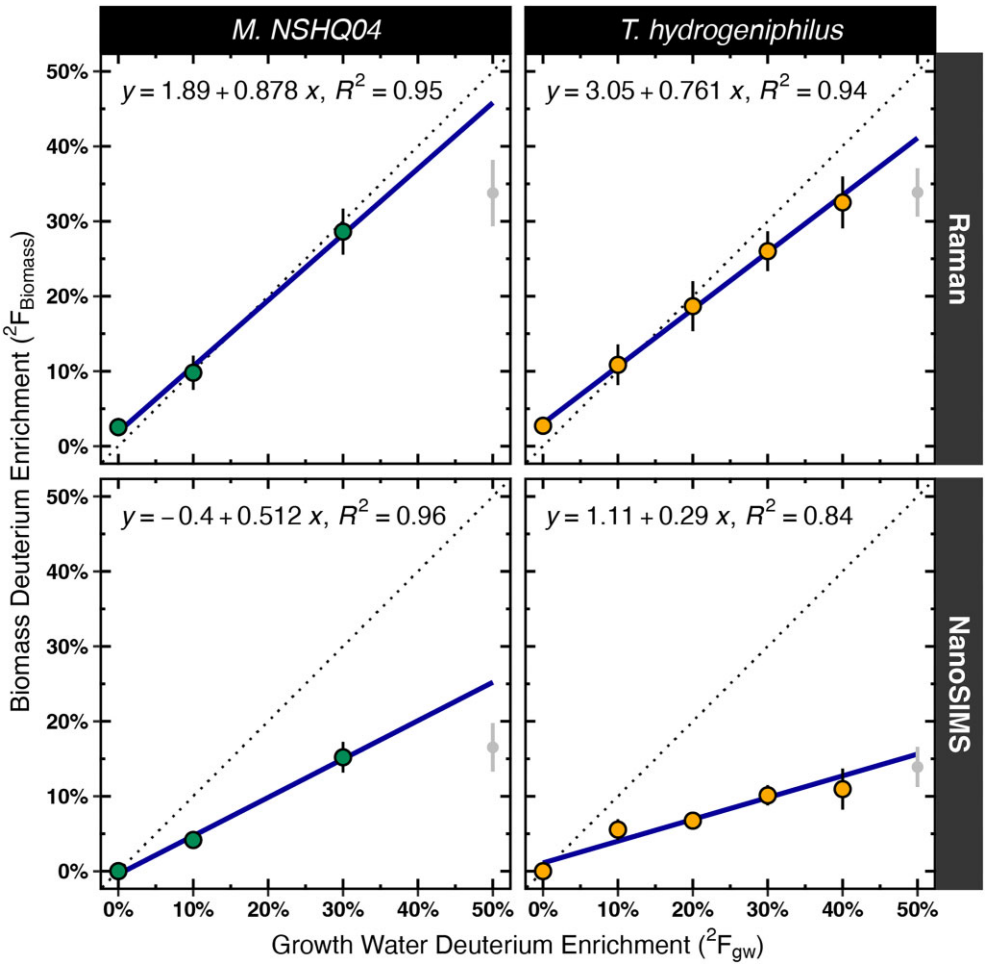

Figure 2. Hydrogen isotope calibrations relating growth water and biomass ^{2}H content. Individual measurements of single-cell biomass deuterium content ($^2F_{biomass}$) conducted with Raman spectroscopy (top panels) or nanoSIMS (bottom panels) are plotted against the corresponding deuterium content of the microbial growth media ($^2F_{gw}$). The dotted line indicates the 1:1 line; the solid line represents the line of best fit whose equation is noted in each panel. Points and error bars displayed are mean and standard deviation of biomass deuterium content, respectively. Note that the linear models displayed in each panel are calculated only with data between deuterium content of 0–40 at. % to ensure that these models are not affected by the toxicity effects observed at 50 at. % label (point intervals in gray).

term defined as the fraction of uncertainty in calculated growth rate over the growth rate itself (σ_μ/μ) where quantifiable growth rate is where relative error = (σ_μ/μ) × 100% <50% (Fig. 3).

The value of the water hydrogen assimilation constant (a_w) was determined for both organisms from the slopes of the linear regression relating $^2F_{biomass}$ versus $^2F_{water}$. This value, $a_w = X_w \times \alpha_{biomass/w}$, corresponds to the isotopic offset between microbial biomass relative to its growth water. This term includes both X_w, the mole fraction of lipid H sourced from growth water, and $\alpha_{biomass/w}$, the isotopic fractionation between whole-cell biomass and growth water (Zhang et al. 2009).

NanoSIMS

Samples were analyzed with a CAMECA NanoSIMS 50 L (CAMECA, Gennevilliers, France) housed in the Caltech Microanalysis Center at the California Institute of Technology. Before, analysis, cells were sputter-coated with 25 nm of Au. Cells were analyzed using a 2.5-pA primary Cs+ beam current, and a presputter time of 6–20 min depending on the size of the raster area. Two masses were collected in parallel ($^1H^-$, $^2H^-$) using electron multipliers. Individual samples were identified using the NanoSIMS CCD camera and correlated with Raman-measurements using previously generated image maps. For all analyses, at least two frames were collected. All ion images were recorded at 512 × 512 pixel area. Single-cell isotope values were quantified using a custom script (see the section "Data availability") relying on the *sims* Python library (https://github.com/zanpeeters/sims). Cell areas were manually defined using the GNU Image Manipulation Program. Isotope ratios (^2R) were converted to fractional abundances (^2F) with the relations: $^2F = {}^2R/(1 + {}^2R)$ and $^2R = {}^2H/{}^1H$, where ^{1}H and ^{2}H represent total ion counts in detectors EM1 and EM2, respectively, averaged across a cell area. Additionally, a deadtime correction (Kilburn and Wacey 2014) was applied: $N = (N_m)/(1–N_m \times \tau/T)$, where N is the real number of secondary ions, N_m is the number of secondary ions measured, τ is deadtime (in seconds), and T is dwell time (seconds per pixel). This instrument's detector deadtime was 44 ns. Deadtime correction had a negligible effect on isotopic values (Supplementary Text, Supplementary Fig. S7).

Results and discussion

Single-cell isotopic measurements

To assess the sensitivity and precision of Raman microspectroscopy as a reporter of cellular ^{2}H incorporation, we generated

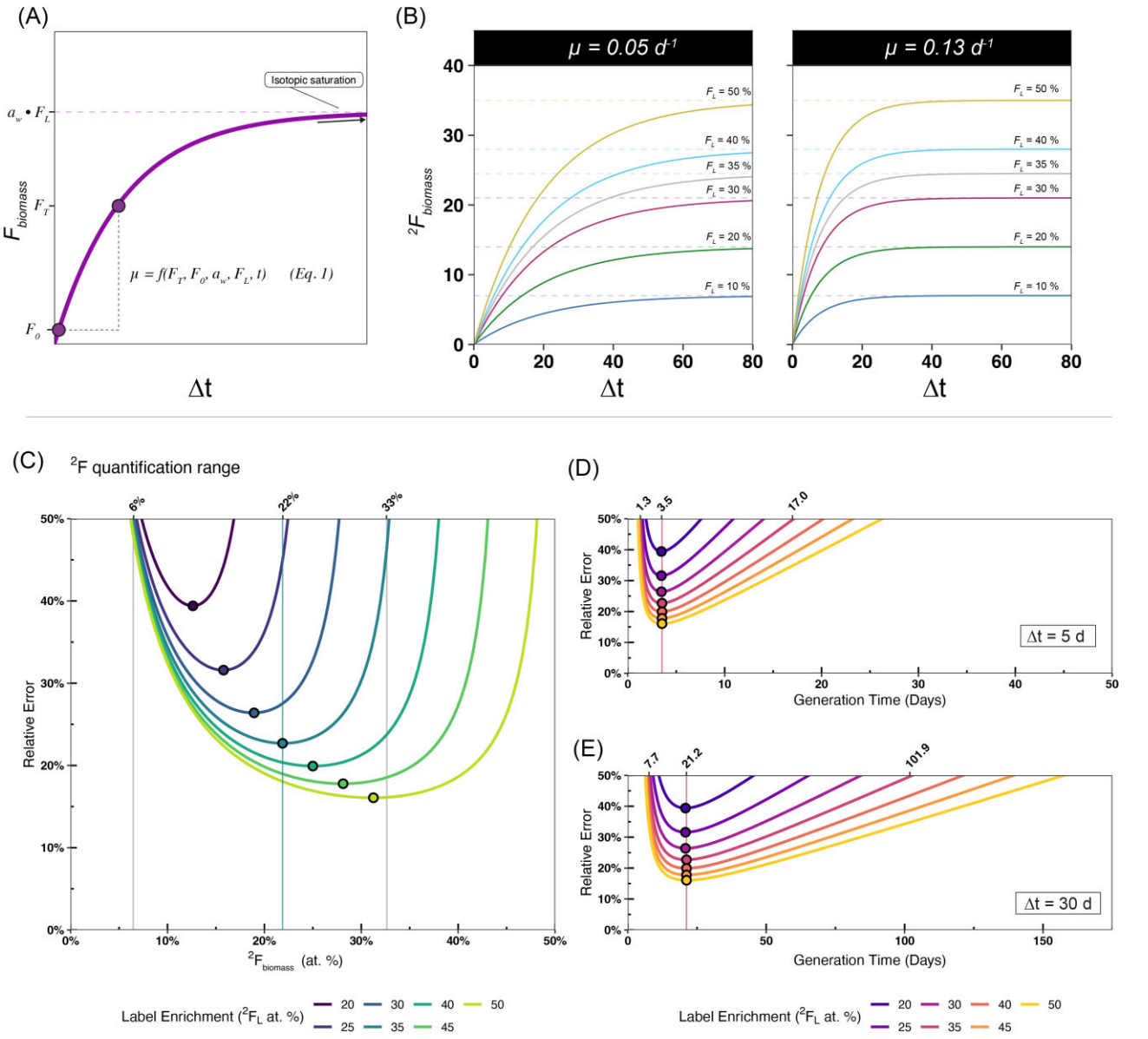

Figure 3. Modeling of microbial growth in the presence of enriched isotopic label (A and B) and associated error in biomass ^2F quantification (C) and growth rate/generation time (D and E). A schematic figure (Panel A) visualizes how microbial growth rate is calculated as a function of biomass isotopic enrichment (F_T), label strength (F_L), incubation time (t), and water assimilation efficiency constant (a_w) (Eq. 1). Similarly, Panel B displays example output of the microbial growth model, where $a_w = 0.7$. Isotopic enrichment increases as a function of time but depends upon isotopic label strength (F_L) and growth rate (μ, noted above each plot). In Panels C–E, we display quantification ranges where relative error in the growth rate measurement is <50% of the growth rate itself (relative error = $\sigma_\mu/\mu \times 100\%$, where μ is apparent growth rate). In Panel C, relative error is plotted against biomass deuterium enrichment ($^2F_{biomass}$) for label strengths ^2F_L ranging from 20 to 50 at. %. Plotted points indicate the of minimum error for each isotopic label. Along the top axis of Panel C, the lower limit, error optimum, and upper limit of quantification, are noted, for the isotopic label strength of $^2F_L = 35$ at. %. The key results from Panel C are summarized in Table 2. In Panels D and E, relative error is plotted against biomass generation times in the context of a simulated SIP incubation. In these examples, the incubation times of 5 days (Panel D) and 30 days (Panel E) are chosen. Along the top axes of Panels D and E, the minimum, optimum, and maximum quantifiable generation times are noted for the isotopic tracer strength of $^2F_L = 35$ at. %. These generation times correspond to the limits of quantification and optima noted in Panel A.

a large isotopic dataset of bacterial and archaeal cells grown to equilibrium with deuterated (^2H_2O) media of varying hydrogen isotope compositions (0–50 at. % ^{2}H). We focused our study on two anaerobic organisms isolated from anaerobic subsurface aquifers: a SRB *T. hydrogeniphilus* (Haouari et al. 2008), and a methanogenic archaeon *Methanobacterium NSHQ04* (Miller et al. 2018). We correlatively acquired individual measurements of cellular deuterium enrichment ($n = 351$) with Raman spectroscopy and nanoSIMS (Fig. 1). We refer to hydrogen isotope content using both Raman and nanoSIMS as the fractional abundance of deuterium, ^2F, reported in atom % (at. %) (see the section "Materials and methods"), where $^2F = {}^2H/(H + {}^2H) \times 100\%$. To generate hydrogen isotope calibrations, we fit simple linear models relating the hydrogen isotopic composition of microbial biomass ($^2F_{biomass}$) to the organism's growth water ($^2F_{gw}$) (Fig. 2).

With Raman microspectroscopy, biomass ^{2}H content ($^2F_{biomass}$) increased linearly and exhibited strong positive correlation ($R^2 =$ 0.94, 0.95, for *T. hydrogeniphilus* and *M. NSHQ04*, respectively) with the ^{2}H content of the growth water ($^2F_{gw}$) (Fig. 2, Table 1B). Raman measurements of biomass deuterium content exhibited an

Table 1. Results and statistical summary of the isotopic calibration. Here, we summarize key outputs of our analyses: (A) analytical uncertainty in biomass measurements across growth water isotopic compositions ($^2F_{gw}$), (B) linear models relating the isotopic composition of biomass ($^2F_{biomass}$) to that of growth water ($^2F_{gw}$), (C) water hydrogen assimilation efficiency factors (a_w) derived from the hydrogen isotopic calibration, with associated standard error, and (D) assessment of correlation between biomass isotopic values estimated with Raman spectroscopy ($^2F_{Raman}$) and nanoSIMS ($^2F_{nanoSIMS}$) (Supplementary Figs S2 and S3).

	Raman	nanoSIMS
(A) Analytical uncertainty in cellular ^2F (SD) (at. %)		
$^2F_{gw}$ = 0% (SD of the method blank)	1.13	0.01
$^2F_{gw}$ = 10%	2.56	1.24
$^2F_{gw}$ = 20%	3.34	1.04
$^2F_{gw}$ = 30%	3.07	2.95
$^2F_{gw}$ = 40%	3.46	2.74
$^2F_{gw}$ = 50%	3.78	3.20
Mean SD across all conditions	2.89	1.86
(B) Hydrogen isotope calibration models		
where: $y = {}^2F_{Biomass}$, $x = {}^2F_{gw}$		
T. hydrogeniphilus	$y = 0.761x + 3.05$ $R^2 = 0.94$	$y = 0.29x + 1.11$ $R^2 = 0.84$
M. NSHQ04	$y = 0.878x + 1.89$ $R^2 = 0.95$	$y = 0.512x–0.40$ $R^2 = 0.96$
(C) Water hydrogen assimilation efficiency		
$a_w \pm SE$		
T. hydrogeniphilus	0.761 ± 0.014	0.290 ± 0.009
M. NSHQ04	0.878 ± 0.020	0.512 ± 0.010
(D) Correlative statistics		
Linear model equation	$y = 0.439x–0.3617$	
where:	Slope SE = 0.01	
$y = {}^2F_{nanoSIMS}$	Intercept SE = 0.24	
$x = {}^2F_{Raman}$		
(Supplementary Text, Supplementary Figs S2 and S3)		
RMSE (at. %)	2.52	

average standard deviation of $\sigma_{2F} = 2.89$ at. %. The variability of Raman-derived $^2F_{biomass}$ increased with the isotopic composition of the growth water: a maximum standard deviation was observed at the $^2F_{gw} = 50\%$ ^2H_2O condition, where $\sigma_{2F} = 3.77$ at. %. Corresponding measurements by nanoSIMS of the same cells followed a similar trend: $^2F_{Biomass}$ increased linearly with the growth water applied ($R^2 = 0.84$, 0.96 for *T. hydrogeniphilus* and *M. NSHQ04*, respectively) and the average standard deviation of nanoSIMS ^2F was $\sigma_{2F} = 1.86$ at. %. Similar to Raman, the standard deviation of nanoSIMS measurements increased along with the isotopic composition of growth water, reaching a maximum at the 50% label where $\sigma_{2F} = 3.20$ at. % (Table 1A). We emphasize that these measures of variance are conservative over-estimates of analytical error due to heterogeneity in the hydrogen isotopic enrichment of individual cells. Our data support previous observations by Berry et al. (2015) that point to high reproducibility of single-cell measurements as we observe a typical analytical uncertainty of less than 1 CD% (Supplementary Text, Supplementary Fig. S11). We apply the larger error term for a more conservative estimation of growth rate measurement range in the proceeding section.

Applying Raman microspectroscopy to SIP growth rate measurements

Having generated a Raman-based hydrogen isotopic calibration of microbial biomass, we sought to test the applicability of this analytical method to measurements of cell-specific growth rate. Microbial growth rate can be inferred from SIP incubations because the degree of an organism's biomass isotopic enrichment over time depends on the isotopic composition of a given substrate and its rate of biomass synthesis (Kopf et al. 2016). Therefore, if measurements of ^2H incorporation are reliable, then these values should translate to cell-specific growth rates. To this end, we sought to parameterize sources of uncertainty and propagation to downstream calculations to define acceptable experimental conditions and analytical uncertainties for quantitative measurement of microbial growth rate.

The growth rate of an organism in the presence of a ^2H_2O is calculated with Eq. (1) (Kopf et al. 2016). In brief, microbial growth rate is a natural logarithmic relationship between an organism's isotopic composition at the start of an incubation (F_0) and its isotopic composition at the time (t) of sampling (F_T). Cellular isotopic enrichment is compared to the enrichment of the isotopic label (F_L) offset by a water hydrogen assimilation efficiency constant (a_w)—a value representing the fraction of biomass hydrogen that a cell acquires from its growth water, as opposed to other metabolic sources and associated fractionation effects.

$$\mu = -\frac{1}{t} \cdot ln\left(\frac{F_T - a_w \cdot F_L}{F_0 - a_w \cdot F_L}\right). \quad (1)$$

We modeled growth rates (μ) (Eq. 1) across a wide range of SIP experimental conditions (varying F_L, t, and a_w,) and applied standard error propagation to determine the associated uncertainty (σ_μ) (Eq. 2) that result from compounding uncertainty of Raman–SIP experimental parameters (Kopf et al. 2016, Caro et al. 2023):

$$\sigma_\mu = \frac{\sqrt{(a_w F_L - F_T)^2 \sigma_{F_0}^2 + (a_w F_L - F_0)^2 \sigma_{F_T}^2 + a_w^2 \cdot (F_0 - F_T)^2 \sigma_{F_L}^2 + F_L^2 \cdot (F_0 - F_T)^2 \sigma_{a_w}^2}}{t \cdot (a_w F_L - F_0) \cdot (a_w F_L - F_T)}, \quad (2)$$

where sigma (σ) terms represent uncertainties of each subscripted parameter (e.g. σ_{FT} represents uncertainty in biomass isotopic composition at time of sampling T). We convert growth rate to

Table 2. Range of Quantification for Raman-derived (CD%-based) measurements of single-cell deuterium content (Fig. 3C). The optimum value represents the $^2F_{biomass}$ value at which relative error in growth rate calculation is minimized. The lower and upper limits of quantification represent where relative error of growth rate calculation exceeds 50%.

Isotopic label strength (^2F_L at. %)	Lower limit of quantification ($^2F_{biomass}$ at. %)	Optimum ($^2F_{biomass}$ at. %)	Upper limit of quantification ($^2F_{biomass}$ at. %)
20	7.4	12.6	16.7
25	6.8	15.8	22.4
30	6.6	18.9	27.7
35	6.4	21.8	32.6
40	6.4	25.0	37.7
45	6.3	28.1	42.8
50	6.2	31.3	48.0

biomass generation time using the relationship:

$$T_G = \frac{\ln(2)}{\mu}, \quad (3)$$

where μ is growth rate in units of t^{-1} and T_G is generation time in units of t.

To a first order, the range of growth rates (μ) that can be measured with SIP depends on the isotopic composition of the label and the incubation duration. Uncertainty in growth rate (σ_μ) depends on uncertainty in label strength (σ_{FL}), biomass isotopic enrichment (σ_{FT}), and microbial water hydrogen assimilation efficiency (σ_{aw}). Our model constrains the region of quantification for both isotopic enrichment (Fig. 3C) and corresponding growth rate (Fig. 3D and E) in Raman SIP experiments. We propagate the uncertainty estimates of $^2F_{biomass}$ estimated from our hydrogen isotope calibration as σ_{FT} to estimate associated uncertainty in growth rate (σ_μ) that results from a given SIP experiment. We report uncertainty in growth rate relative to the growth rate itself as *Relative Error* $= (\sigma_\mu/\mu) \times 100\%$. We set our limit for relative error to be 50% such that errors below this cutoff result in growth rate differences that are distinguishable with $>2\sigma$ confidence.

In Fig. 3, we display example outputs from our model using incubation times of $t = 5$ days and $t = 30$ days across a range of ^2H_2O label strengths. For example, the range of quantification for an experiment applying a 35% label is 6.9–32.6 at. % deuterium enrichment. Ranges of quantification and error optima for additional isotopic label strengths are reported in Table 2. For a 5-day incubation, this range of ^2F quantification corresponds to growth rates between 0.53 and 0.04 d^{-1}, or generation times of 1.3 and 17 days. For a 30-day incubation, this range of ^2F quantification corresponds to growth rates between 0.09 and 0.007 d^{-1} or generation times between 7.7 and 101.9 days (Fig. 3E).

Asymptotic rises in uncertainty at high and low biomass isotopic enrichment, respectively, correspond to (i) uncertainty in growth rate as cell isotopic enrichment approaches that of the label solution and (ii) uncertainty resulting from biomass isotopic signal not significantly exceeding that of the noise inherent to the analytical method. The first condition (i) represents cells that grow faster than can be discriminated using the set incubation time and label strength, while (ii) represents cells that grow too slowly to be distinguished from noise. It should be noted that our ranges of quantification should be viewed conservative estimates, as the source of uncertainty we apply corresponds to heterogeneity of ^2H-incorporation across cell populations, as opposed to the error across individual Raman acquisitions. This latter source of error is far smaller both in our dataset and in previously reported datasets (Berry et al. 2015) (Supplementary Fig. S11).

Incubation time (t) shifts the dynamic range of SIP (Supplementary Fig. S8): shorter incubations can resolve faster-growing organisms from each other but may not capture slower-growing organisms due to insufficient label incorporation. Conversely, longer incubations can capture slower-growing organisms, but faster-growing organisms may become saturated with the label and will no longer be resolvable from each other (Fig. 3). Growth rates of fast-growing organisms, those that are readily saturated with deuterium, could lead to underestimates of aggregate microbial turnover.

Increasing the strength of the label (F_L) expands the dynamic range of the SIP method i.e. both slower and faster growth rates can be captured as there is more isotopic "space" that can be measured (Table 2, Fig. 3). However, increasing F_L must be weighed against the risk that higher deuterium concentrations can impose toxicity or unintended physiological effects. Deuterated water at high levels of isotopic labeling have been shown to have no effect, inhibition and even stimulation among different microorganisms (Lester et al. 1960, Berry et al. 2015, Kopf et al. 2015). In our experiments, we observed depressed isotopic enrichment in growth water containing 50 at. % ^2H_2O. These effects were noted for both organisms and both the Raman and nanoSIMS data (gray point intervals in Fig. 2). We suspect that this result stems from isotopic toxicity affecting microbial growth or metabolic switching at high isotopic enrichment. Deuterium toxicity may result from decreased reaction rate of deuterium relative to protium and by physiological stress induced by altered solvent characteristics. Recent molecular dynamics analyses suggest that ^2H_2O as a solvent can have profound impacts on lipid membrane packing and protein organization (Tempra et al. 2023). Thus, it is conceivable that increased protein and membrane rigidity at high ^2H_2O concentrations inhibits growth, induces metabolic switching (i.e. acquiring more H from nonwater sources) or stress responses. We emphasize that the exact mechanism of D_2O toxicity cannot be explained by our study and that more targeted studies of deuterium toxicity mechanisms are warranted. We caution against applying ^2H_2O label strengths at or above 50 at. % due to varying physiological effects that may arise at this threshold, especially when applying this approach to natural microbial communities of unknown and mixed composition. In addition, we encourage future researchers applying ^2H_2O–SIP at high concentrations to include an unlabeled control to monitor changes in physiology, metabolite production, transcription, and so on. Uncertainties in isotopic label strength (σ_{FL}) due to pipetting or gravimetric dilution contribute relatively minor components to total uncertainty, especially at high isotopic enrichment. Unintended evaporation of a water-based tracer may lead to increased uncertainty in label strength via the different evaporation rates of deuterated and nondeuterated water. Evaporative effects would contribute to a gradual isotopic enrichment of the growth medium in a manner predicted by a Rayleigh distillation model. Thus, though isotopic distillation can be numerically modeled, conducting water-based SIP in a closed system is preferable for many experimental designs.

The water hydrogen assimilation efficiency constant (a_w) is essential for estimation of microbial growth rate, as it sets the upper limit of biomass deuterium enrichment. This limit is represented by the $a_w \cdot F_L$ terms in Eq. (1) (Fig 3A). Therefore, similar to increasing the strength of the label, an organism with a greater a_w has more isotopic "space" in which to become enriched. In our

study, we use Raman-derived ^2F measurements to empirically determine the a_w of *T. hydrogeniphilus* and *M. NSHQ04* to be $a_w = 0.76 \pm 0.02$ and $a_w = 0.88 \pm 0.02$, respectively (Table 1C, Fig. 2). The higher a_w observed with the methanogen *M. NSHQ04* is in line with primarily autotrophic growth (Miller et al. 2018) with an offset from $a_w = 1$ due to hydrogen isotopic fractionation. The slightly lower a_w for the sulfate reducing *T. hydrogeniphilus* is indicative of a hydrogen contribution from its acetotrophic metabolism. This result supports prior observations by Berry et al. (2015) who noted substantial differences in ^{2}H incorporation between heterotrophs and autotrophs arising from differences in hydrogen sources between organisms and metabolisms. We note that Raman-derived values represent a_w of whole-cell biomass, which may be distinct from those calculated via compound-specific analysis (Zhang et al. 2009, Wijker et al. 2019, Caro et al. 2023). It was previously reported that uncertainty in a_w is a significant driver of uncertainty in hydrogen SIP-derived growth rate estimates (Caro et al. 2023). In studies of mixed communities, this uncertainty must be propagated through growth rate calculations. For organisms with known metabolisms, the a_w term can be estimated as common metabolic modes often constrain a_w factor to a degree (Zhang et al. 2009, Wijker et al. 2019, Caro et al. 2023). In an ideal scenario, this uncertainty would be constrained or minimized by prior knowledge of dominant metabolisms present in an environmental sample (e.g. via marker gene or metagenomic sequencing).

Raman and nanoSIMS measure different pools of cellular hydrogen

Deuterium abundances measured by Raman were greater than those measured by nanoSIMS when compared to the culture growth water (Fig. 2). When we correlated cell-specific $^2F_{biomass}$ measurements we observed that, cell-to-cell, nanoSIMS-derived hydrogen isotope values were severely depressed compared to corresponding Raman-derived values (Supplemental Fig. S2). A depression in expected isotopic content relative to an expected value can be expressed as a dilution factor, where the decrease in isotope abundance is expressed as a percentage. From this correlative dataset, we calculated an average approximate hydrogen isotope dilution factor of 58.7 ± 6.0% across all growth water labeling conditions (Supplementary Text).

Depression of isotopic enrichment measured by nanoSIMS due to sample preparation has been widely reported for multiple stable isotope tracers (^{13}C, ^{18}O, ^{15} N, ^{2}H, and ^{34}S) under various preparation conditions, as stains, fixatives, and nucleic acid probes can overprint cellular isotopic signals (Musat et al. 2014, Kopf et al. 2015, Pernice et al. 2015, Woebken et al. 2015, Stryhanyuk et al. 2018, Meyer et al. 2021). Our results point to a separate phenomenon: the replacement of exchangeable hydrogen during sample washing. Such a significant dilution of deuterium abundance speaks to a fundamental difference in the nature of nanoSIMS- and Raman-based measurements. Owing to how the primary ion beam ionizes and ablates a cell, nanoSIMS is mostly agnostic to the sources of ^{2}H/^{1}H it measures, setting aside potential differences in hydrogen ionization efficiency across different classes of molecules. Therefore, $^1H^-$ and $^2H^-$ ions reaching the instrument detectors can derive from a variety of cellular hydrogen sources including relict cytosolic water, adsorbed extracellular water, and biomass hydrogen in both nonexchangeable sites and exchangeable sites that are readily mixed with natural-abundance washing buffers during sample preparation. Protonated sites in biomolecules (e.g. O–H, N–H, S–H, and so on) experience rapid exchange with aqueous wash solutions on the order of picoseconds to minutes (Bai et al. 1993, Englander et al. 1996), meaning that anabolically produced O–^{2}H, N–^{2}H, S–^{2}H, and so on bonds would be rapidly overprinted by natural-abundance hydrogen during washing procedures (Fig. 4). As described in the section "Materials and methods," no stains or probes were applied to the cells in this study. Therefore, the hydrogen dilution factors reported here result primarily from sample washing. This significant and persistent isotopic dilution may confound efforts to use deuterium tracers as measures of biosynthesis in nanoSIMS-based studies (Kopf et al. 2015). This problem is compounded at lower-isotopic enrichment, where substantial variability in ^{2}H/^{1}H values results from low ^{2}H ion counts as well as variation in which cell subcomponents (which may display distinct ^{2}H enrichments) are ablated (Kopf et al. 2015). Preparatory methods that forego or reduce washing may suffer from an opposite effect: protic sites in microbial biomass, still in isotopic equilibrium with the ^{2}H-enriched growth medium, could contribute to a biomass ^{2}H/^{1}H in excess of what was generated through anabolic processes. Future work should apply caution when applying dilution factors to back-calculate isotopic abundance, as these can vary widely between the sample preparation and organism (Meyer et al. 2021), an effect that may be pronounced in environmental systems with mixed microbial communities.

A key advantage of Raman–SIP is that the C–H (2800–3100 cm^{-1}) and C–D (2040–2300 cm^{-1}) bands report solely nonexchangeable carbon–hydrogen and carbon–deuterium stretching modes associated with mostly lipids, proteins, and nucleic acids (Berry et al. 2015, Cui et al. 2022). These spectral regions are oblivious to exchangeable bonding environments including O–H, N–H, S–H, and so on, as well as relict water. Raman microspectroscopy, therefore focuses on anabolically produced organic bonds without confounding hydrogen sources. It is important to note that the application of organic nucleic acid probes, such as stains, FISH, or CARD-FISH, as well as organic fixatives such as formaldehyde, may interfere with Raman-derived measurements via the introduction of nonbiomass C–H bonds (Berry et al. 2015) (Supplementary Text, Supplementary Fig. S9). Therefore, despite the utility linking microbial identity to function, the application of nucleic acid probes to both Raman–SIP and nanoSIMS–SIP studies may be unsuitable for optimum quantification of microbial growth. However, because of its nondestructive nature, Raman can be readily applied as a mid-point, rather than end-point analysis, and so the application of FISH or stains after Raman measurement is plausible.

Future directions and limitations for Raman–SIP

Because Raman microspectroscopy is a standard technique for mineralogical/material characterization, it brings with it several aspects that complement SIP practices. First, it is a nondestructive, rapid method. Like nanoSIMS, Raman is readily coregistered with other techniques such as fluorescence microscopy, FISH, scanning electron microscopy, or cell sorting (Berry et al. 2015, Schaible et al. 2022). A single Raman spectrum takes between seconds to 1 min to acquire, and many Raman instruments are equipped with epifluorescence modules that can enable simultaneous visualization of cells in addition to transmitted or reflected light microscopy. Second, Raman is comparatively accessible relative to nanoSIMS and allows analysis with minimal preparation, foregoing the need for conductive surfaces and/or metallic sputter coating, vacuum chamber, and secondary electron optics. Raman instruments like those employed in this study are similar in operation to epifluorescence microscopes, which lowers user

(A)

Bond Type	Formula	Measured by SIMS?	Measured by Raman*?
Carbon H	$-CH_x$	Yes	Yes
Water H	H_2O	Yes	No
Protic H	-O-H	Yes	No
	$-N-H_x$	Yes	No
	-S-H	Yes	No

*in the high wavenumber region 2000 - 3100 cm^{-1}

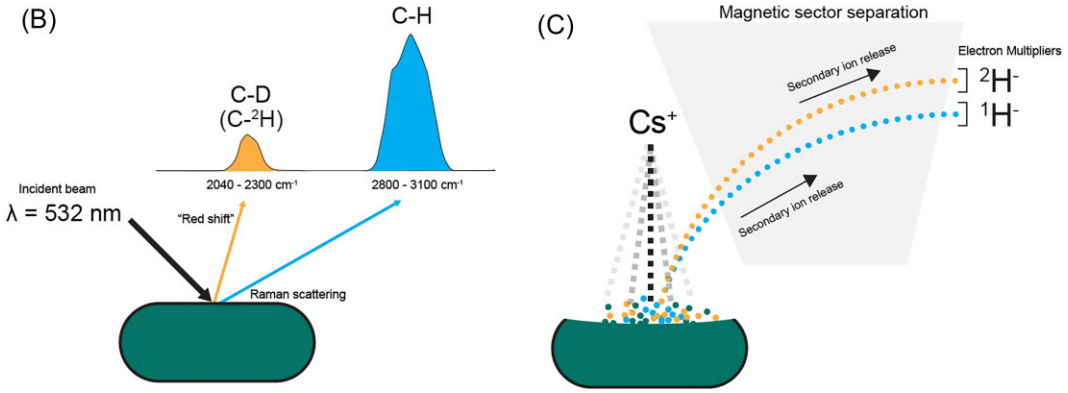

Figure 4. Schematic diagram showing the dilution of ^{2}H/H isotopic signal due to sample preparation, and how Raman and nanoSIMS measure different pools of biomass ^{2}H/H. (A) The original pool of deuterated cell mass is biosynthesized, sourcing ^{2}H from the growth medium. During sample washing, hydrogen in exchangeable, or "protic" bonding environments rapidly exchange with wash solutions, leaving a diluted residual pool of ^{2}H/H. Carbon–hydrogen and carbon–deuterium bonds are not affected by this dilution effect, as ^{2}H/H in these bonds do not exchange during washing. (B) Within the C–H and C–D (C–^{2}H) wavenumber regions, Raman is only sensitive to carbon–hydrogen and carbon–deuterium bonds, which are not affected by dilution due to washing, whereas (C) nanoSIMS ostensibly measures all pools of ^{2}H/H, including those affected by dilution.

barrier-to-entry and improves the capacity for direct deployment on various forms of environmental samples including filters, rock faces, plant material, and so on. Third, Raman microspectroscopy has microscale spatial resolution and provides diagnostic information about cellular organic composition. The fingerprint region (200–1800 cm^{-1}) can identify specific biomolecular composition (Cui et al. 2022), which can be useful for differentiating taxa and growth stage (Supplementary Fig. S1) (Mosier-Boss 2017, Novelli-Rousseau et al. 2018, Wang et al. 2020). Fourth, the Raman fingerprint region enables identification of biologically precipitated minerals and the mineralogical/material context of a cell (Klein et al. 2015, Suzuki et al. 2020). Raman SIP with deuterium, specifically, makes identification of individual cell and mineral components in organic–mineral assemblages feasible because the C–D band occupies a typically silent region in inorganic Raman spectra. Coregistered mineral and cell-activity measurements can support investigations into the cell–mineral and cell–cell relationships that drive microbial activity (Templeton and Caro 2023).

Despite the promise of Raman SIP, this method has key caveats that must be considered and/or addressed. The major disadvantage of ^{2}H–Raman–SIP is sensitivity. Classical or spontaneous Raman microspectroscopy of microbial cells is limited by low signal intensities, particularly in samples with high autofluorescence (Hatzenpichler et al. 2020). A key outcome of our study is the definition of Raman–SIP ranges of quantification for growth rate estimation. Our results conservatively define the minimum cutoff for quantitative growth rate measurement as ~7 at. % (Table 2), depending on the label strength applied. Microbial ^{2}H incorporation that does not exceed this threshold cannot be quantitatively distinguished from noise. Similarly, microbial ^{2}H incorporation in excess of the upper range of quantification cannot yield quantitative growth rates. We emphasize that our estimates of uncertainty (and by extension, growth rate quantification ranges) should serve as guidelines and we encourage future researchers to estimate these parameters for their own instruments and experiments. Further computational tool development and optimization may further improve Raman's detection limit and growth rate quantification capabilities (Schaible et al. 2024).

While we have demonstrated severe dilution of hydrogen isotopic measurements by nanoSIMS, this methodology remains well-suited to sensitively measure isotopes of C, N, O, S, and so on at the single-cell level. While measurement of ^{13}C and ^{15}N has been demonstrated with Raman, the precision of these measurements is far below that of nanoSIMS and is traceable only within specific biomolecules (Cui et al. 2017, Weber et al. 2021). In the coming years, advancements in Raman technology and data processing (Schaible et al. 2024) could conceivably increase sensitivity and subsequently improve isotopic measurements. Specifically, surface- or tip-enhanced Raman spectroscopy (Efrima and Zeiri 2009, Mosier-Boss et al. 2016, Chisanga et al. 2017, 2018, Mosier-Boss 2017), stimulated Raman scattering, resonance Raman spectroscopy, or coherent anti-Stokes Raman spectroscopy, which are shown to improve acquisition times and enhance signal, could be evaluated for isotopic measurements (Ivleva et al. 2010, 2017, Camp and Cicerone 2015, Kubryk et al. 2015, Cicerone 2016, Cui et al. 2017, Chisanga et al. 2018, Hu et al. 2019, Weiss

et al. 2019). However, at present, validation of these methods for SIP is required (Supplementary Text, Supplementary Figs S4 and S5). As noted earlier, Raman–SIP may suffer dilution effects related to staining or the use of nucleic acid probes (FISH), similar to nanoSIMS. Similarly, fixatives such as formaldehyde, in stabilizing the cell membrane, introduce C–H bonds that can affect isotopic measurements (Supplementary Text, Supplementary Fig. S9).

Compared to the surveys of microbial identity and functional potential, relatively few measurements of cellular growth rates in nature exist (Koch et al. 2018, Caro et al. 2023, Templeton and Caro 2023, Foley et al. 2024). Growth rates of microorganisms in complex systems can inform theories of microbial ecology, as well as elucidate preferences of microbial taxa for specific environmental niches, substrates, and microscale locality. In the rock-hosted biosphere, for example, measurements of microbial anabolic activity can clarify how microbial activity relates to mineralogical context, or how the activities of microbial partners/consortia are correlated. While we present a calibration of environmentally relevant taxa, further validation of Raman–SIP and correlative measurements of mineralogical/material composition is required in complex environmental samples.

For the benefit of future researchers, we designed an interactive GUI, *Shiny R-SIP*, that allows users to implement our SIP model and optimize their experiments by considering how the relevant sources of uncertainty impact the design of a Raman–SIP experiment (Supplementary Data or online: https://apps.kopflab.org/login with login credentials username: *shiny-rSIP*, password: *public-access*). The GUI allows users to adjust parameters of label strength, incubation time, and water–hydrogen assimilation efficiency, as well associated uncertainties in these terms, in order to design effective SIP experiments. The parameters we define in our microbial growth model are specific to the study organisms used and our Raman instrument—they are intended to provide reasonable estimates of uncertainty that may be encountered. Users of this GUI are encouraged to define their own uncertainty terms by constraining the technical variation in individual CD% measurements inherent to their Raman instrument. For samples where microbial growth may exhibit large variation, we suggest users consider multiple incubation times (or subsampling efforts) to effectively capture a wide range of biomass growth rates in experiments targeting natural microbial communities, while also quantifying their threshold of tracer saturation as an upper-limit of growth-rate quantification.

Conclusions

In this work, we provide the basis for the quantitative measurement of single-cell microbial growth rates via Raman–SIP. We develop hydrogen isotope calibrations for two organisms, *T. hydrogeniphilus* (sulfate-reducing bacterium) and *M. NSHQ04* (methanogenic archaeon). These calibrations validate the utility of Raman microspectroscopy as a method for measuring microbial $^{2}H/^{1}H$ enrichment. Applying our Raman-derived isotopic calibration to a model of microbial growth, we define ranges of quantification for Raman SIP experiments where single-cell growth rates can be sensitively distinguished. We find that with reasonable (20–40 at. % $^{2}H_2O$) isotopic label strengths and incubation times, Raman–SIP can capture a wide array of microbial generation times, with this range being defined by the parameters of the SIP experiment. These ranges of quantification can guide the design and interpretation of SIP experiments where Raman is used to track cellular ^{2}H incorporation. Finally, we observe that hydrogen isotopic values derived from nanoSIMS suffer from severe dilution resulting from the rapid exchange of protic H in aqueous solution. Raman-based methodology avoids this issue because its analytical windows exclusively target carbon-bound hydrogen. In conclusion, this work provides a robust framework for applying deuterium Raman–SIP to spatially resolved, quantitative investigations of microbial activity in environmental and model systems.

Acknowledgements

We would like to thank the University of Colorado Boulder, Department of Geological Sciences for support of this study. The authors sincerely thank Yunbin Guan of the Caltech Microanalysis Center for expertise with nanoSIMS measurements. We thank Eric Ellison of the CU Boulder Raman Microspectroscopy Laboratory (RRID: SCR_019305) for assistance with Raman measurements and data analysis. We extend sincere thanks to John Magyar for valuable discussions during the design of this study. We credit Dan Utter for assistance with nanoSIMS data processing and initial drafting of the nanoSIMS data extraction script. We thank Rebecca Wipfler for assistance with laser microdissection microscopy and coupon etching.

Author contributions

Tristan A. Caro (Conceptualization, Data curation, Formal analysis, Investigation, Methodology, Software, Validation, Visualization, Writing – original draft, Writing – review & editing), Srishti Kashyap (Conceptualization, Data curation, Formal analysis, Investigation, Methodology, Resources, Writing – original draft, Writing – review & editing), George Brown (Formal analysis), Claudia Chen (Formal analysis), Sebastian H. Kopf (Funding acquisition, Software, Supervision, Writing – review & editing), and Alexis S. Templeton (Funding acquisition, Project administration, Resources, Supervision, Writing – review & editing)

Supplementary data

Supplementary data is available at *FEMSEC Journal* online.

Conflict of interest: None declared.

Funding

This work was also supported by a NASA Exobiology Program grant to A.T. (80NSSC21K0489) and an Army Research Office grant to S.K. (W911NF2120119/78484-LS). T.C. was supported by a National Science Foundation Graduate Research Fellowship and through the BioFrontiers Institute of the University of Colorado Boulder. C.C. and G.B. were supported by the Laboratory for Interdisciplinary Statistical Analysis at the University of Colorado Boulder. The Laboratory for Interdisciplinary Statistical Analysis at the University of Colorado Boulder is supported by National Science Foundation grant number 1955109.

Data availability

Raw data collected for this study is archived at https://osf.io/rqk27/. Raw data, processed data, and analysis scripts used to process data and generate visualizations are available at https://github.com/tacaro/Caro-et-al-Raman-SIP. The interactive GUI referenced in this manuscript is available at https://apps.kopflab.org/login with login username *shiny-rSIP* and password *public-access*. In

addition, the GUI can be downloaded for local use from the manuscript GitHub repository.

References

Bai Y, Milne JS, Mayne L *et al.* Primary structure effects on peptide group hydrogen exchange. *Proteins* 1993;**17**:75–86.

Berry D, Mader E, Lee TK *et al.* Tracking heavy water (D_2O) incorporation for identifying and sorting active microbial cells. *Proc Natl Acad Sci USA* 2015;**112**:E194–203.

Boetius A, Ravenschlag K, Schubert CJ *et al.* A marine microbial consortium apparently mediating anaerobic oxidation of methane. *Nature* 2000;**407**:623–6.

CAMECA. A selection of CAMECA NanoSIMS users. 2024. https://www.cameca.com/company/links/nanosims. (22 May 2024, date last accessed).

Camp CH, Cicerone MT. Chemically sensitive bioimaging with coherent Raman scattering. *Nature Photon* 2015;**9**:295–305.

Caro TA, McFarlin J, Jech S *et al.* Hydrogen stable isotope probing of lipids demonstrates slow rates of microbial growth in soil. *Proc Natl Acad Sci USA* 2023;**120**:e2211625120.

Casar CP, Kruger BR, Flynn TM *et al.* Mineral-hosted biofilm communities in the continental deep subsurface, Deep Mine Microbial Observatory, SD, USA. *Geobiology* 2020;**18**:508–22.

Chisanga M, Muhamadali H, Ellis DI *et al.* Surface-enhanced raman scattering (SERS) in microbiology: illumination and enhancement of the microbial world. *Appl Spectrosc* 2018;**72**:987–1000.

Chisanga M, Muhamadali H, Kimber R *et al.* Quantitative detection of isotopically enriched *E. coli* cells by SERS. *Farad Discuss* 2017;**205**:331–43.

Cicerone M. Molecular imaging with CARS micro-spectroscopy. *Curr Opin Chem Biol* 2016;**33**:179–85.

Cordero OX, Ventouras LA, DeLong EF *et al.* Public good dynamics drive evolution of iron acquisition strategies in natural bacterioplankton populations. *Proc Natl Acad Sci USA* 2012;**109**:20059–64.

Coskun ÖK, Özen V, Wankel SD *et al.* Quantifying population-specific growth in benthic bacterial communities under low oxygen using $H_2{}^{18}O$. *ISME J* 2019;**13**:1546–59.

Cui D, Kong L, Wang Y *et al.* In situ identification of environmental microorganisms with Raman spectroscopy. *Environ Sci Ecotechnol* 2022;**11**:100187.

Cui L, Yang K, Zhou G *et al.* Surface-enhanced Raman spectroscopy combined with stable isotope probing to monitor nitrogen assimilation at both bulk and single-cell level. *Anal Chem* 2017;**89**:5793–800.

Cui L, Yang K, Zhu YG. Stable isotope-labeled single-cell Raman spectroscopy revealing function and activity of environmental microbes. In: Dumont MG, Hernández García M (eds), *Stable Isotope Probing: Methods and Protocols*. New York: Springer, 2019, 95–107. https://doi.org/10.1007/978-1-4939-9721-3_8.

Dekas AE, Parada AE, Mayali X *et al.* Characterizing chemoautotrophy and heterotrophy in marine archaea and bacteria with single-cell multi-isotope NanoSIP. *Front Microbiol* 2019;**10**. https://www.frontiersin.org/articles/10.3389/fmicb.2019.02682.

Dumont MG, Murrell JC. Stable isotope probing—linking microbial identity to function. *Nat Rev Micro* 2005;**3**:499–504.

Ebrahimi A, Schwartzman J, Cordero OX. Cooperation and spatial self-organization determine rate and efficiency of particulate organic matter degradation in marine bacteria. *Proc Natl Acad Sci USA* 2019;**116**:23309–16.

Efrima S, Zeiri L. Understanding SERS of bacteria. *J Raman Spectrosc* 2009;**40**:277–88.

Eichorst SA, Strasser F, Woyke T *et al.* Advancements in the application of NanoSIMS and Raman microspectroscopy to investigate the activity of microbial cells in soils. *FEMS Microbiol Ecol* 2015;**91**:fiv106. https://doi.org/10.1093/femsec/fiv106.

Englander SW, Sosnick TR, Englander JJ *et al.* Mechanisms and uses of hydrogen exchange. *Curr Opin Struct Biol* 1996;**6**:18–23.

Foley M, Stone BWG, Caro TA *et al.* Microbial growth in soil. *EcoEvoRxiv* 2024. https://ecoevorxiv.org/repository/view/7290/.

Grossart HP, Kiørboe T, Tang K *et al.* Bacterial colonization of particles: growth and interactions. *Appl Environ Microb* 2003;**69**:3500–9.

Haouari O, Fardeau ML, Cayol JL *et al.* *Thermodesulfovibrio hydrogeniphilus* sp. nov., a new thermophilic sulphate-reducing bacterium isolated from a Tunisian hot spring. *Syst Appl Microbiol* 2008;**31**:38–42.

Hatzenpichler R, Krukenberg V, Spietz RL *et al.* Next-generation physiology approaches to study microbiome function at single cell level. *Nat Rev Micro* 2020;**18**:241–56.

Hu F, Shi L, Min W. Biological imaging of chemical bonds by stimulated Raman scattering microscopy. *Nat Methods* 2019;**16**:830–42.

Hungate BA, Mau RL, Schwartz E *et al.* Quantitative microbial ecology through stable isotope probing. *Appl Environ Microb* 2015;**81**:7570–81.

Ivleva NP, Kubryk P, Niessner R. Raman microspectroscopy, surface-enhanced Raman scattering microspectroscopy, and stable-isotope Raman microspectroscopy for biofilm characterization. *Anal Bioanal Chem* 2017;**409**:4353–75.

Ivleva NP, Wagner M, Horn H *et al.* Raman microscopy and surface-enhanced Raman scattering (SERS) for in situ analysis of biofilms. *J Biophotonics* 2010;**3**:548–56.

Kellermann MY, Wegener G, Elvert M *et al.* Autotrophy as a predominant mode of carbon fixation in anaerobic methane-oxidizing microbial communities. *Proc Natl Acad Sci USA* 2012;**109**:19321–6.

Kilburn MR, Wacey D. CHAPTER 1. Nanoscale secondary ion mass spectrometry (NanoSIMS) as an analytical tool in the geosciences. In: *Principles and Practice of Analytical Techniques in Geosciences*. London: Royal Society of Chemistry, 2014, 1–34.

Kirchman DL. Growth rates of microbes in the oceans. *Annu Rev Mar Sci* 2016;**8**:285–309.

Klein F, Humphris SE, Guo W *et al.* Fluid mixing and the deep biosphere of a fossil Lost City-type hydrothermal system at the Iberia Margin. *Proc Natl Acad Sci USA* 2015;**112**:12036–41.

Koch BJ, McHugh TA, Hayer M *et al.* Estimating taxon-specific population dynamics in diverse microbial communities. *Ecosphere* 2018;**9**:e02090.

Kopf SH, McGlynn SE, Green-Saxena A *et al.* Heavy water and 15 N labelling with NanoSIMS analysis reveals growth rate-dependent metabolic heterogeneity in chemostats. *Environ Microbiol* 2015;**17**:2542–56.

Kopf SH, Sessions AL, Cowley ES *et al.* Trace incorporation of heavy water reveals slow and heterogeneous pathogen growth rates in cystic fibrosis sputum. *Proc Natl Acad Sci USA* 2016;**113**:E110–6.

Kubryk P, Kölschbach JS, Marozava S *et al.* Exploring the potential of stable isotope (Resonance) Raman microspectroscopy and surface-enhanced Raman scattering for the analysis of microorganisms at single cell level. *Anal Chem* 2015;**87**:6622–30.

Lester W, Sun SH, Seber A. Observations on the influence of deuterium on bacterial growth. *Ann NY Acad Sci* 1960;**84**:667–77.

Li J, Mau RL, Dijkstra P *et al.* Predictive genomic traits for bacterial growth in culture versus actual growth in soil. *ISME J* 2019;**13**:2162–72.

Marlow J, Spietz R, Kim KY *et al.* Spatially resolved correlative microscopy and microbial identification reveal dynamic depth- and

mineral-dependent anabolic activity in salt marsh sediment. *Environ Microbiol* 2021;**23**:4756–77.

Meyer NR, Fortney JL, Dekas AE. NanoSIMS sample preparation decreases isotope enrichment: magnitude, variability and implications for single-cell rates of microbial activity. *Environ Microbiol* 2021;**23**:81–98.

Miller HM, Chaudhry N, Conrad ME *et al.* Large carbon isotope variability during methanogenesis under alkaline conditions. *Geochim Cosmochim Acta* 2018;**237**:18–31.

Morono Y, Terada T, Nishizawa M *et al.* Carbon and nitrogen assimilation in deep subseafloor microbial cells. *Proc Natl Acad Sci USA* 2011;**108**:18295–300.

Mosier-Boss PA, Sorensen KC, George RD *et al.* SERS substrates fabricated using ceramic filters for the detection of bacteria. *Spectrochim Acta Part A* 2016;**153**:591–8.

Mosier-Boss PA. Review on SERS of bacteria. *Biosensors* 2017;**7**:51.

Musat N, Stryhanyuk H, Bombach P *et al.* The effect of FISH and CARD-FISH on the isotopic composition of 13C- and 15N-labeled *Pseudomonas putida* cells measured by nanoSIMS. *Syst Appl Microbiol* 2014;**37**:267–76.

Novelli-Rousseau A, Espagnon I, Filiputti D *et al.* Culture-free antibiotic-susceptibility determination from single-bacterium Raman spectra. *Sci Rep* 2018;**8**:3957.

Pernice M, Dunn SR, Tonk L *et al.* A nanoscale secondary ion mass spectrometry study of dinoflagellate functional diversity in reef-building corals. *Environ Microbiol* 2015;**17**:3570–80.

Schaible GA, Cliff JB, Crandall JA *et al.* Comparing Raman and NanoSIMS for heavy water labeling of single cells [Internet]. *BioRxiv* 2024. https://www.biorxiv.org/content/10.1101/2024.07.05.602271v1.

Schaible GA, Kohtz AJ, Cliff J *et al.* Correlative SIP–FISH–Raman–SEM–NanoSIMS links identity, morphology, biochemistry, and physiology of environmental microbes. *ISME Commun* 2022;**2**:1–10.

Sokol NW, Slessarev E, Marschmann GL *et al.* Life and death in the soil microbiome: how ecological processes influence biogeochemistry. *Nat Rev Micro* 2022;**20**:1–16.

Stryhanyuk H, Calabrese F, Kümmel S *et al.* Calculation of single cell assimilation rates from SIP-NanoSIMS-derived isotope ratios: a comprehensive approach. *Front Microbiol* 2018;**9**. https://www.frontiersin.org/articles/10.3389/fmicb.2018.02342.

Suzuki Y, Yamashita S, Kouduka M *et al.* Deep microbial proliferation at the basalt interface in 33.5–104 million-year-old oceanic crust. *Commun Biol* 2020;**3**:1–9.

Templeton AS, Caro TA. The rock-hosted biosphere. *Annu Rev Earth Planet Sci* 2023;**51**:493–519.

Tempra C, Chamorro VC, Jungwirth P. Effects of water deuteration on thermodynamic and structural properties of proteins and biomembranes. *J Phys Chem B* 2023;**127**:1138–43.

Trembath-Reichert E, Morono Y, Ijiri A *et al.* Methyl-compound use and slow growth characterize microbial life in 2-km-deep subseafloor coal and shale beds. *Proc Natl Acad Sci USA* 2017;**114**:E9206–15.

Trembath-Reichert E, Shah Walter SR, Ortiz MAF *et al.* Multiple carbon incorporation strategies support microbial survival in cold subseafloor crustal fluids. *Sci Adv* 2021;**7**:eabg0153.

Védère C, Vieublé Gonod L, Nunan N *et al.* Opportunities and limits in imaging microorganisms and their activities in soil microhabitats. *Soil Biol Biochem* 2022;**174**:108807.

Wang K, Chen L, Ma X *et al.* Arcobacter identification and species determination using Raman spectroscopy combined with neural networks. *Appl Environ Microb* 2020;**86**:e00924–20.

Weber F, Zaliznyak T, Edgcomb VP *et al.* Using stable isotope probing and Raman microspectroscopy to measure growth rates of heterotrophic bacteria. *Appl Environ Microb* 2021;**87**:e01460–21.

Wegener G, Kellermann MY, Elvert M. Tracking activity and function of microorganisms by stable isotope probing of membrane lipids. *Curr Opin Biotechnol* 2016;**41**:43–52.

Weiss R, Palatinszky M, Wagner M *et al.* Surface-enhanced Raman spectroscopy of microorganisms: limitations and applicability on the single-cell level. *Analyst* 2019;**144**:943–53.

Wijker RS, Sessions AL, Fuhrer T *et al.* 2H/1H variation in microbial lipids is controlled by NADPH metabolism. *Proc Natl Acad Sci USA* 2019;**116**:12173–82.

Woebken D, Burow LC, Behnam F *et al.* Revisiting N_2 fixation in Guerrero Negro intertidal microbial mats with a functional single-cell approach. *ISME J* 2015;**9**:485–96.

Zhang X, Gillespie AL, Sessions AL. Large D/H variations in bacterial lipids reflect central metabolic pathways. *Proc Natl Acad Sci USA* 2009;**106**:12580–6.

Received 22 January 2024; **revised** 12 July 2024; **accepted** 5 August 2024